



Influence of different complexing agents on structural, morphological, and magnetic properties of Mg–Co ferrites synthesized by sol–gel auto-combustion method

Lichao Yu¹ and Aimin Sun^{1,2,*}

¹College of Physics and Electronic Engineering, Northwest Normal University, Lanzhou 730070, China

²Key Laboratory of Atomic and Molecular Physics & Functional Materials of Gansu Province, Lanzhou 730070, China

Received: 1 December 2020

Accepted: 6 March 2021

Published online:
20 March 2021

© The Author(s), under exclusive licence to Springer Science+Business Media, LLC, part of Springer Nature 2021

ABSTRACT

In the preparation process of magnesium-cobalt nano-ferrite powder ($\text{Mg}_{0.1}\text{Co}_{0.9}\text{Fe}_2\text{O}_4$) by sol–gel self-propagation method, the effect of complexing agent on the nanostructure and magnetic properties of ferrite is studied by changing the type of complexing agent (the complexing agent includes citric acid, oxalic acid, tartaric acid, glucose, and egg white). The XRD pattern of each sample has eight distinct characteristic peaks, and the number of the strongest peak in each map is one [i.e., (311) peak]. All these evidences can preliminarily indicate that the sample has a spinel structure. In addition, in the FTIR of the sample, it can be seen that there are several distinct characteristic peaks at 580 cm^{-1} (i.e., Fe–O peak, etc.) which can also prove the structural characteristics of the sample. In the SEM map, the sample can be seen to have an elliptical shape with a crystalline grain size between 28 and 50 nm. From this, we can guess that the complexing agent participates in the reaction and has a certain influence on the particle size of the sample. Elemental analysis showed that all the six samples prepared contained magnesium, cobalt, iron, and oxygen, and then we quantitatively analyzed the sample to find that the prepared sample was the target product. The BET test shows that a sample is prepared with glucose as the complexing agent, the specific surface area of it can be increased. The VSM data show that magnesium–cobalt ferrite powder with high saturation magnetization, residual magnetization, and coercivity can be prepared by selecting glucose as the complexing agent.

Address correspondence to E-mail: sunam@nwnu.edu.cn

1 Introduction

The production of magnetic materials has a long history [1, 2]. This material has been widely used in electric power, telecommunications and automatic control with pure iron (99.9% Fe), ferrosilicon alloy (Si-Fe, also known as silicon steel) and iron-nickel alloys (Fe-Ni, also known as permalloy) as typical representatives of such materials. Pure iron (also known as engineering pure iron) has been used in electrical technology as a metallic magnetic material before the nineteenth century. However, it was replaced by various types of ferromagnetic alloys in the early twentieth century because the resistivity of pure iron is too small and the loss of eddy current is too large [3, 4]. The resistivity of ferrosilicon alloy is several times higher than pure iron, and ferrosilicon alloy is the most commonly used magnetic materials for generator, motor, and some transformers with high power [5–7]. Iron-nickel alloy has superior high-frequency magnetic characteristics than ferrosilicon alloy, so it opens up new possibilities for metal magnetic materials to be used as special transformers in submarine cables, televisions, precision instruments, etc. [8], and as recording heads, such as recording and video recording field in the applications of high frequency. For general pure iron and ferrosilicon alloys, the eddy current generated inside the material will cause a significant loss of energy when the frequency of utilization is increased, thus making its application in high frequency very limited. Metallic magnetic material, such as silicon steel, is generally rolled into a sheet whose thickness is between 0.05 and 0.1 mm and then superimposed to be a high-frequency transformer which makes the process complicated and costly. Due to the urgent requirements of high-frequency radio technology, the development of non-metallic magnetic materials have increased rapidly, and their application has not been limited to the high-frequency range for a long time.

Ferrite is a composite oxide composed of iron and one or more other metals. For example, the chemical formula of the spinel ferrite is MeFe_2O_4 , or $\text{Me-O-Fe}_2\text{O}_3$, where Me is a divalent metal ion which has an ionic radius similar to that of the ferric ion Fe^{2+} (e.g., Mn^{2+} , Zn^{2+} , Cu^{2+} , Ni^{2+} , M^{2+} , Co^{2+} , etc.) or a group of various metal ions whose average chemical price is divalent (e.g., $\text{Ni}_{0.56}\text{Fe}_{0.44}$). Both MnFe_2O_4 and ZnFe_2O_4 are ferrites replaced by one kind of metal

ion, and sometimes are referred to as a one-component ferrite. In order to meet different magnetic characteristics, ferrites replaced by two or more metal ions are called two-component ferrites or multi-component ferrites [9, 10]. For example, frequently-used manganese-zinc ferrite ($\text{Mn-ZnFe}_2\text{O}_4$) and nickel-zinc ferrite ($\text{Ni-ZnFe}_2\text{O}_4$) are two-component ferrites, while manganese-magnesium-zinc ferrite ($\text{Mn-Mg-ZnFe}_2\text{O}_4$) is a multi-component ferrite. The magnetic properties of ferrite also appear to have a high magnetic permeability at high frequencies, whose metal magnetic material, such as permalloy and alumino-silicon-iron alloy, cannot match. In the production process, the ferrite is similar to the general ceramic process, whose operation is convenient and easy to control, and it is not necessary, like a metal magnetic material, to be rolled into a thin sheet or made into a fine powder medium.

The general nature of spinel ferrite nanoparticles is to change their performance to meet the requirements by changing the synthesis process, precursor pH, catalyst ion substitution, annealing conditions, agglomeration, and the like [3, 4, 11, 12]. In this experiment, the sample was prepared by sol-gel auto-ignition method, and the type of complexing agent was changed during the experiment to explore the effect of complexing agent on the nanostructure and magnetic properties of ferrite. The structural properties of the samples were characterized by X-ray diffraction (XRD) and Fourier transform infrared spectroscopy (FTIR), and then the microstructure of the sample was observed by a scanning electron microscope (SEM). Energy-dispersive X-ray (EDS) is used to determine the chemical elements and the ration of it in the sample. The BET test shows that when preparing a sample with glucose as a complexing agent, the specific surface area of the sample can be increased. The vibrating sample magnetometer (VSM) tested the magnetic properties of the ferrite samples to determine which complexing agent had a greater effect on the magnetic properties of the prepared samples.

2 Experimental process

In the experiment of preparing magnesium-cobalt nano-ferrite powder ($\text{Mg}_{0.1}\text{Co}_{0.9}\text{Fe}_2\text{O}_4$) by sol-gel self-propagation method, the variety of complexing agent is changed. The complexing agents are citric

acid, oxalic acid, tartaric acid, glucose, and egg white. The chemical raw materials are magnesium nitrate $[\text{Mg}(\text{NO}_3)_2 \cdot 6\text{H}_2\text{O}]$, cobalt nitrate $[\text{Co}(\text{NO}_3)_2 \cdot 6\text{H}_2\text{O}]$, ferric nitrate $[\text{Fe}(\text{NO}_3)_3 \cdot 9\text{H}_2\text{O}]$, glucose ($\text{C}_6\text{H}_{12}\text{O}_6$), citric acid ($\text{C}_6\text{H}_8\text{O}_7 \cdot \text{H}_2\text{O}$), tartaric acid ($\text{C}_4\text{H}_6\text{O}_6$), oxalic acid ($\text{C}_2\text{H}_2\text{O}_4$), and egg whites. Metal nitrates and different complexing agents (egg white, tartaric acid, EDTA, oxalic acid, and citric acid) were accurately weighed and dissolved in distilled water. The optimum molar ratio of metal cation to citric acid, glucose, tartaric acid, and oxalic acid in the precursor solution is 1:1.3, and the best ratio of ferrite sample prepared with egg white as complexing agent is 20 ml of the fresh protein and 100 ml of the distilled water whose mixture is as precursor solution. The mixture was stirred uniformly by a glass rod, until there was no visible matter. During the mixing process, aqueous ammonia solution was gradually added to obtain a solution whose pH was 3. The evenly mixed precursor solution was heated and stirred at 80 °C for 3 to 4 h in a thermostatic magnetic heater to form the uniform and stable wet gel. Subsequently, the wet gel was dried in a drying oven at 120 °C for 2 h to obtain a dry gel. The morphology of the dried gel is shown in Fig. 1, and the dried sample was ignited to heat the porcelain bowl to obtain a silver-gray powder. The finally obtained gel was heated at a constant temperature in a tube furnace at 650 °C for 3 h, and then the sintered powder was ground for half an hour to obtain a sample.

3 Results and discussion

3.1 Structural characterization

The XRD map of the magnesium–cobalt ferrite sample prepared with different complexing agent is presented in Fig. 2. We know that metal cations can still undergo complexation reactions without the use of complexing agents in the experiment. Each sample has eight distinct characteristic peaks as shown in Fig. 2 [i.e., (311), (111), (220), (222), (400), (422), (511), and (440)] which proves that the sample can still form a spinel structure without the use of a complexing agent [13]. However, a small peak appears at around 35° and we know that the peak is Fe_2O_3 phase by searching literature [14, 15]. The main reason of the appearance of the impurity peak is that the complexation reaction among the metal cations is

incomplete without complexing agent. The map of each sample corresponds more perfect to the standard card of CoFeO_4 (JCPDS No. 22-1086), so it can be concluded that the prepared sample is a ferrite material with a spinel structure. We can also see the appearance of impurity peaks on the sample map of the reaction with complexing agent, which may be due to the fact that the complexing agent is also a combustion improver in this experiment. Different complexing agents have different effects on the complexation reaction of ions, resulting in different degrees of complexation reaction. In addition, comparing the peak intensities of the different samples, it can be seen that different complexing agents also affect the crystallization of the sample [16]. When we use glucose as a complexing agent and a combustion improver, the sample has the strongest crystallinity, which may be caused by annealing at 650 °C. The most suitable annealing temperature required for the sample prepared with glucose as a complexing agent is similar, that is, the energy required for crystallization of the sample can be provided at 650 °C. Due to the presence of magnesium–cobalt ferrite itself in the form of Fe^{3+} and Fe^{2+} , the energy required for the remaining samples to anneal is quite different. The excess energy oxidizes Fe^{2+} to Fe^{3+} , and Fe^{3+} ions precipitate out during the cooling process to form Fe_2O_3 . Some XRD diffraction peaks of the magnesia–cobalt ferrites prepared using different complexing agents is weak and wide. The reason may be that the disordered intercrystalline structure of magnesium–cobalt ferrite nanocrystals and the defects in the nanocrystals cause continuous changes in lattice spacing.

Reading the XRD pattern of six samples with jade 6.5 gives the specific position of the sample (311) peak, the interplanar spacing, and half width. We combine these data with the following formula and get the parameters to describe the microstructure of the sample, such as plane spacing (d), lattice constant (a), crystalline grain size (D), unit volume unit (a^3), and dislocation line density (δ). Detailed data are shown in Tables 1 and 2.

The application formula is as follows:

Specific values of lattice constants can be obtained by the following formula [17]:

$$a = d\sqrt{h^2 + k^2 + l^2}, \quad (1)$$

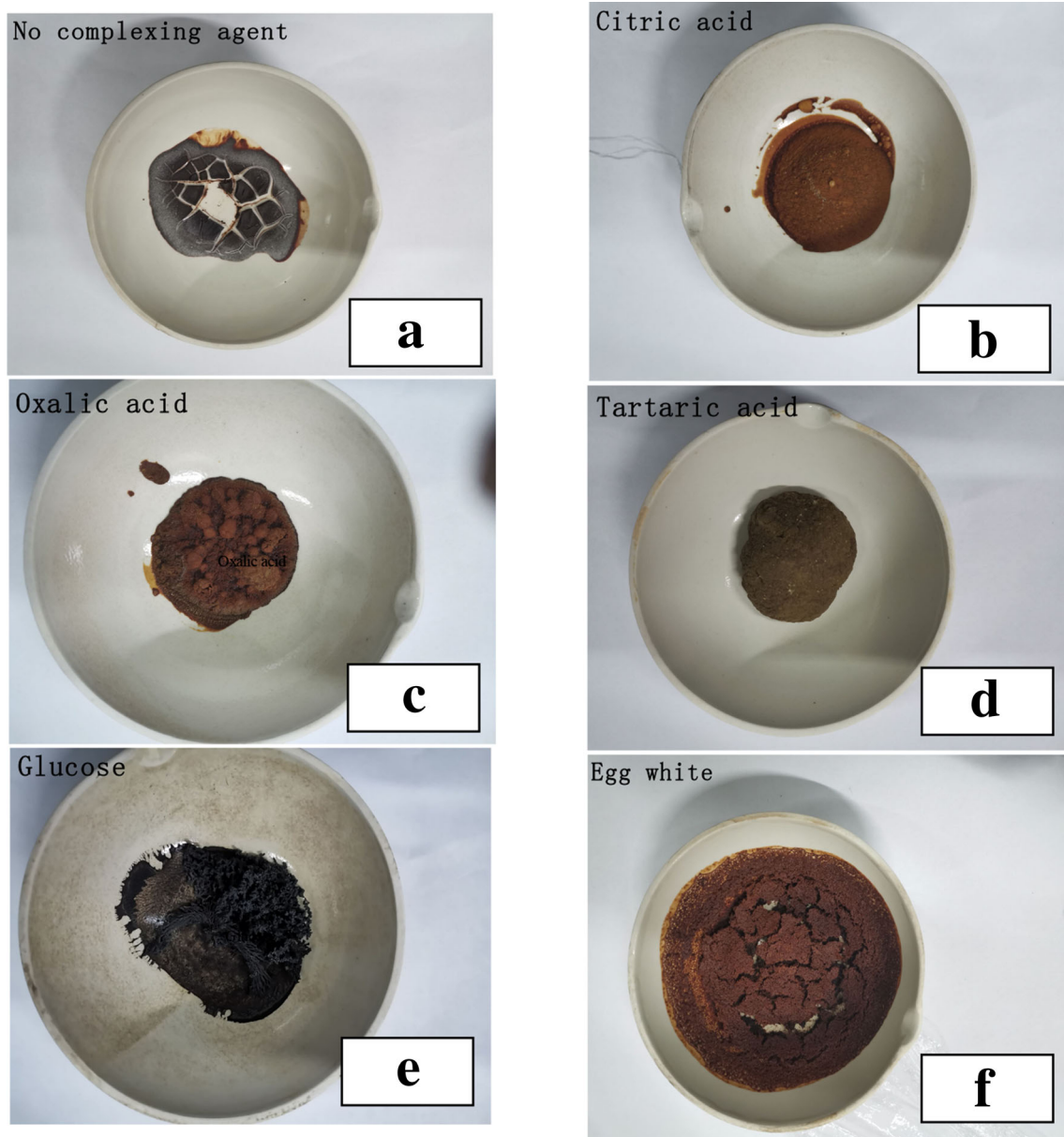


Fig. 1 The appearance of dry gelatin

where $(h\ k\ l)$ is the Miller index and d is the plane spacing.

The average particle size can be calculated by the following formula [18]:

$$D = \frac{0.9\lambda}{\beta \cos \theta}. \quad (2)$$

The dislocation line density is calculated by the following formula [19]:

$$\delta = \frac{1}{D^2}, \quad (3)$$

where D is the average crystallite size, λ is the wavelength of X-ray, β is the full width at half maximum of the diffraction peak, and θ is the Bragg angle of the peak position of the main peak.

The X-ray density ρ_x , the bulk density ρ_b , and the porosity P were calculated by the following formula. The calculated values for the different contents are listed in Table 2. ρ_x , ρ_b , and P can be calculated by the following formula [20]:

Fig. 2 (Color online) X-ray powder diffraction for $Mg_{0.1}Co_{0.9}Fe_2O_4$ ferrite nanoparticles prepared using different complexing agents

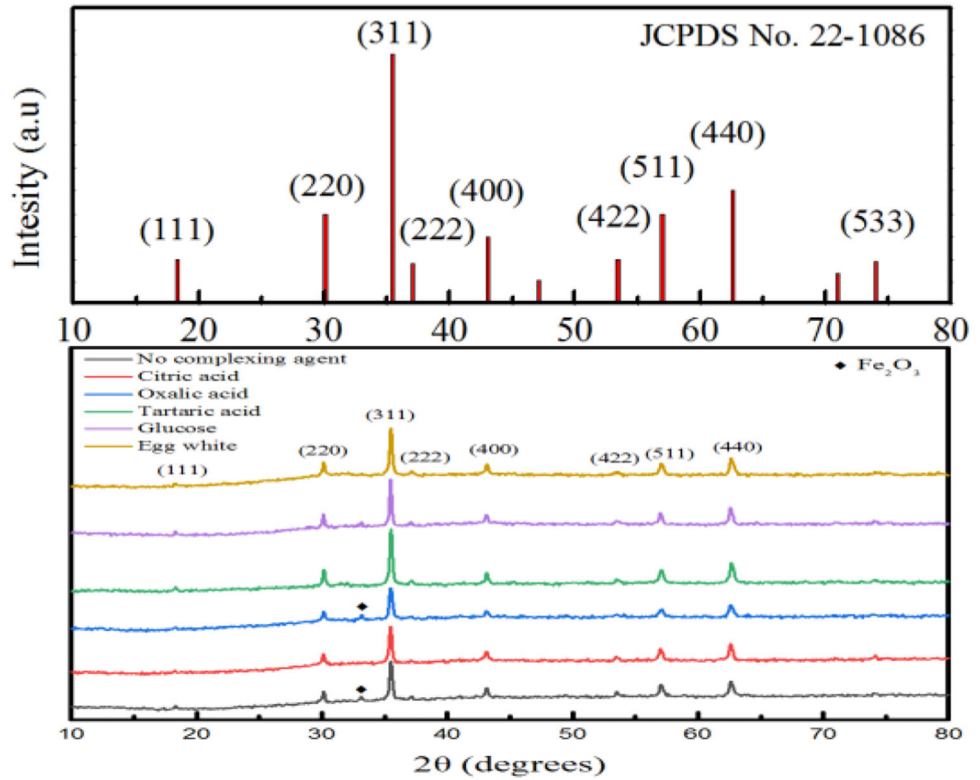


Table 1 Parameters obtained from XRD data of $Mg_{0.1}Co_{0.9}Fe_2O_4$ nano-ferrite particles prepared from different complexing agents

Complexing agent	Inter planar spacing, d (Å)	Lattice constant, a (Å)	Particle size, D (nm)	Volume of unit cell, a^3 (Å ³)	Dislocation line density, δ (10^{-3} nm^{-2})
No complexing agent	2.5276	8.3831	33.10	589.13	0.91
Citric acid	2.5239	8.3681	33.50	585.98	0.89
Oxalic acid	2.5283	8.3854	29.78	589.62	1.12
Tartaric acid	2.5246	8.3731	38.98	587.03	0.66
Glucose	2.5283	8.3854	46.33	589.62	0.47
Egg white	2.5258	8.3771	34.61	587.87	0.83

Table 2 Various structural parameters of $Ni_{0.2}Cu_{0.1}Co_{0.7}Fe_2O_4$ nano-ferrite particles

Complexing agent	X-ray density, ρ_x (kg/m ³)	Tetrahedral site, d_A (Å)	Octahedral site, d_B (Å)
No complexing agent	5214.47	3.6300	2.9639
Citric acid	5242.51	3.6234	2.9586
Oxalic acid	5210.14	3.6310	2.9647
Tartaric acid	5233.12	3.6256	2.9603
Glucose	5210.13	3.6310	2.9647
Egg white	5225.65	3.6274	2.9618

$$\rho_x = \frac{8M}{N_A a^3}, \tag{4}$$

where M is the relative molecular mass of samples when the doping amount x in ferrites is equal to different values. In general calculation, N_A is

Avogadro constant and its numerical value is usually 6.02×10^{23} .

The following relationship is used to calculate the A (tetrahedral) and B (octahedral) sites of the magnetic ion (hopping length) and the distance between them [16]:

$$d_A = \frac{\sqrt{3}}{4}a, \quad (5)$$

$$d_B = \frac{\sqrt{2}}{4}a. \quad (6)$$

By calculation, as shown in Table 1, the lattice constant of the sample also changes due to the difference of complexing agent, which may be attributed to the fact that the sintering temperatures required for each sample are different with different complexing agents as combustion improvers. In other words, when the complexing agent is different, the energy required for crystallization of the sample is different. When the energy supplied is lower than the required energy, the growth of the sample is insufficient and then it causes the change in lattice constant. When the energy is higher than the required energy, the excess energy causes the ferrous ions in the ferrites to oxidize to ferric ions and then it causes lattice deformation; thus, the lattice constant changes. Samples prepared with different complexing agents (glucose, oxalic acid, protein, tartaric acid, and citric acid) have different average grain sizes. The average grain size of different complexing agents from small to large is in the following order: oxalic acid, no complexing agent, citric acid, egg white, tartaric acid, and glucose, and the specific values are shown in Table 1. When glucose is used as the complexing agent, the sample has the largest particle which may be due to the same change trend of the ferrite particle size and the degree of polymerization of the carbohydrate organic complexing agent. At the same calcination temperature, the organic complexing agent which has a larger molecular size and a longer chain length can prepare ferrite whose particles are larger. The organic complexing agent which has a larger molecular size and a longer chain length allows the ferrite particles to grow faster under the same change of temperature. In addition, in Tables 1 and 2, it can be seen that the parameters of the unit volume unit (a^3) and the dislocation line density (δ) also vary due to changes in the lattice constant.

3.2 Fourier transform infrared spectroscopy (FTIR)

The Fourier transform infrared spectrum of the magnesium–cobalt ferrite powder prepared by different complexing agents (citric acid, oxalic acid, tartaric acid, glucose, and egg white) is shown in Fig. 3. The type of functional group of the sample and the crystal structure determine the position and intensity of the absorption peak. Since the positions of the metal cations in the crystal lattice are different, the bond lengths of the ferric ions and the ions are different. This difference leads to the difference of the frequency of the vibration of the Fe–O [21], and then the positions of the absorption peaks are different. It is shown in the figure that each sample has several distinct absorption peaks, such as ν_1 , 1640 cm^{-1} , 1384 cm^{-1} , and 1132 cm^{-1} [22]. The position of the ν_1 absorption peak is between 570 and 596 cm^{-1} (specific peaks are shown in Table 3). It is a characteristic peak of the functional group formed by the oxygen ion and the Fe^{3+} ion (at the octahedral position). The absorption peak at around 1640 cm^{-1} is a characteristic peak of hydroxide, the absorption peak at around 1384 cm^{-1} is the characteristic peak of nitrate, and the absorption peak at around 1130 cm^{-1} is the characteristic peak of C–O bond. The absorption peak of the functional group formed by Fe^{3+} and oxygen ions in the tetrahedral position was not found in the map because its vibration frequency exceeded the measurement range of the instrument. The presence of these absorption peaks also confirmed that the prepared samples all had a spinel structure.

However, in the absorption spectrum of the powder which is from self-propagating combustion of the xerogel, it can be seen that the spectrum exhibits typical characteristics of the IR spectrum of a typical inorganic substance. After annealing at $650 \text{ }^\circ\text{C}$, the characteristic peaks of $-\text{COOH}$ and NO_3^- almost disappeared completely in the spectrum, and a strong absorption peak appeared at around 582 cm^{-1} , which corresponds to the characteristic absorption peak of Fe–O ferrite. It indicates that the self-propagating combustion reaction occurred between the nitrate and the carbon-containing group. The nitrate has oxidizing property to be as an oxidizing agent, and the carbon-containing group acts as a reducing agent in the reaction. A redox reaction occurs between them and a large amount of heat is released. The heat causes the Fe–O ferrite to form the

Fig. 3 FT-IR spectra of $Mg_{0.1}Co_{0.9}Fe_2O_4$ ferrite nanoparticles prepared using different complexing agents

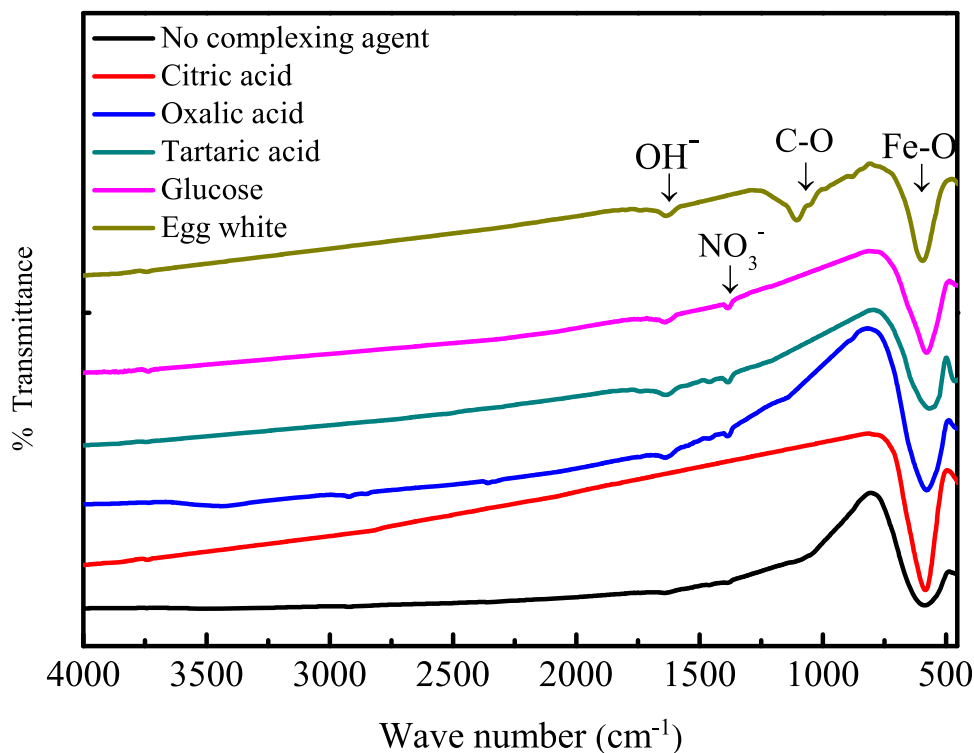


Table 3 Frequency bands ν_1 of the samples

Complexing agent	Sample	Annealing temperature (°C)	ν_1 (cm ⁻¹)
No complexing agent	$Mg_{0.1}Co_{0.9}Fe_2O_4$	650	586
Citric acid	$Mg_{0.1}Co_{0.9}Fe_2O_4$	650	584
Oxalic acid	$Mg_{0.1}Co_{0.9}Fe_2O_4$	650	578
Tartaric acid	$Mg_{0.1}Co_{0.9}Fe_2O_4$	650	570
Glucose	$Mg_{0.1}Co_{0.9}Fe_2O_4$	650	579
Egg white	$Mg_{0.1}Co_{0.9}Fe_2O_4$	650	596

spinel structure instantaneously during the self-combustion process. The complexing agent used in this experiment mainly plays two roles in the reaction. Firstly, it acts as a complexing agent to form a uniform, stable and transparent sol in the early stage of the reaction; secondly, it acts as a fuel to provide energy for the self-combustion reaction. It is shown in Table 3 that the absorption peak ν_1 also moves with different complexing agents, and the change is the most pronounced when tartaric acid is used as the complexing agent. It indicates that the addition of the complexing agent can affect the bond length of the Fe–O bond and then can change the frequency of the vibration. It also provides a powerful reference for studying the influence of the type of complexing agent on the microstructure of magnesium–cobalt ferrite.

3.3 Scanning electron microscopy (SEM)

Figure 4 shows a photograph of a sample topography taken by a scanning electron microscope of each sample. From the SEM photograph of the product, it is known magnesium–cobalt ferrite particles have small particle sizes, good dispersibility, and uniform size. Due to the strong magnetic properties of the sample, the phenomenon of particle agglomeration is serious. But, the basic morphology of the sample particles can still be clearly seen. The sample particles are round or oval, and the particle size is between 20 and 50 nm, which indicates that the complexing agent has a certain effect on the particle size of magnesium–cobalt ferrite.

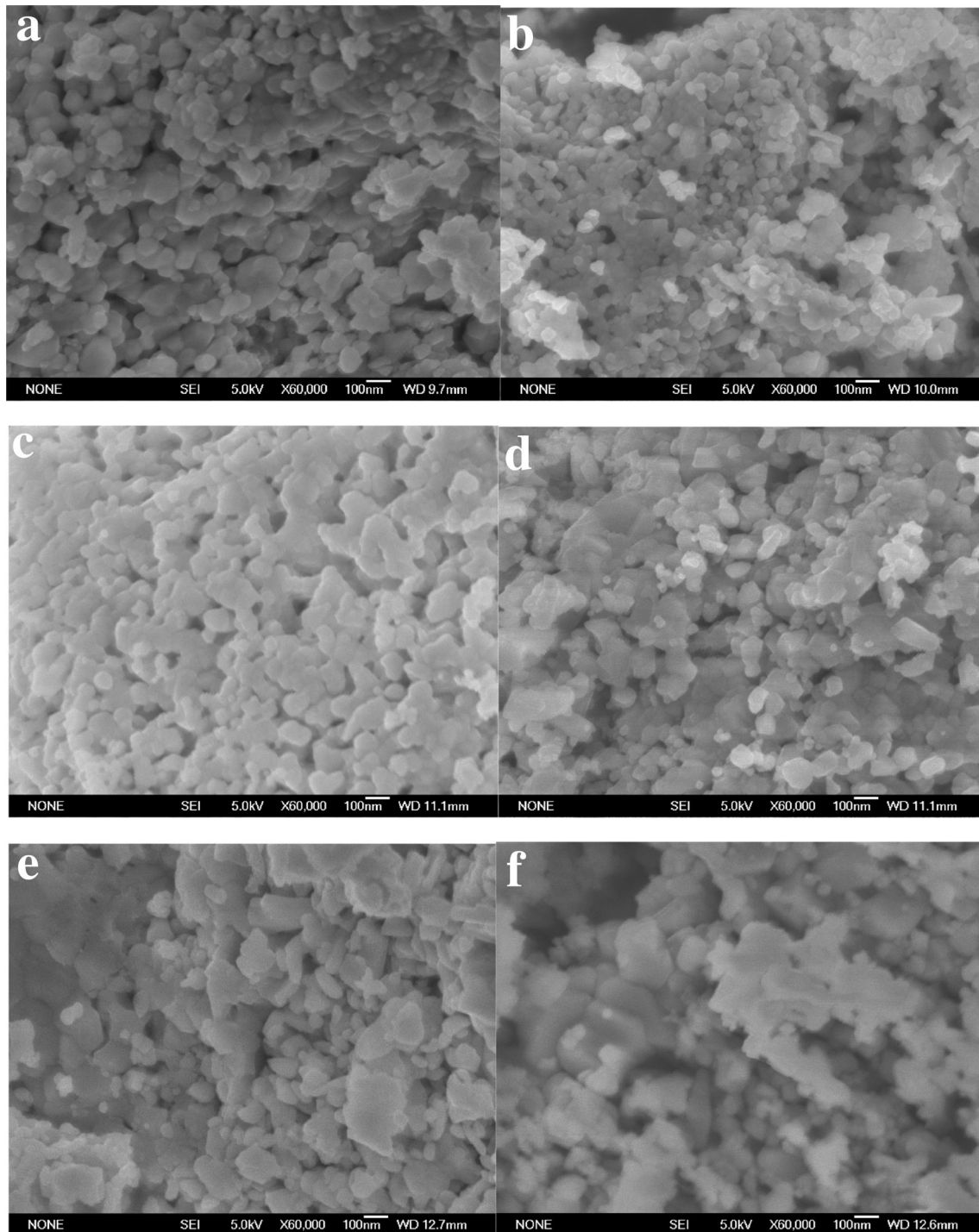


Fig. 4 Scanning electron microscopy micrographs of $\text{Ni}_{0.2}\text{Mg}_{0.1}\text{Co}_{0.9}\text{Fe}_2\text{O}_4$ ferrite nanoparticles prepared using different complexing agents: **a** no complexing agent, **b** citric acid, **c** oxalic acid, **d** tartaric acid, **e** glucose, and **f** egg white

3.4 Elemental analysis (EDS)

The above can prove the successful preparation of magnesium–cobalt ferrite powder with spinel structure using different complexing agents and

combustion improvers (citric acid, oxalic acid, tartaric acid, glucose, and egg white). This is mainly due to the use of egg white as the complexing agent. The same sample was selected from multiple regions to quantitatively analyze the sample, and the average

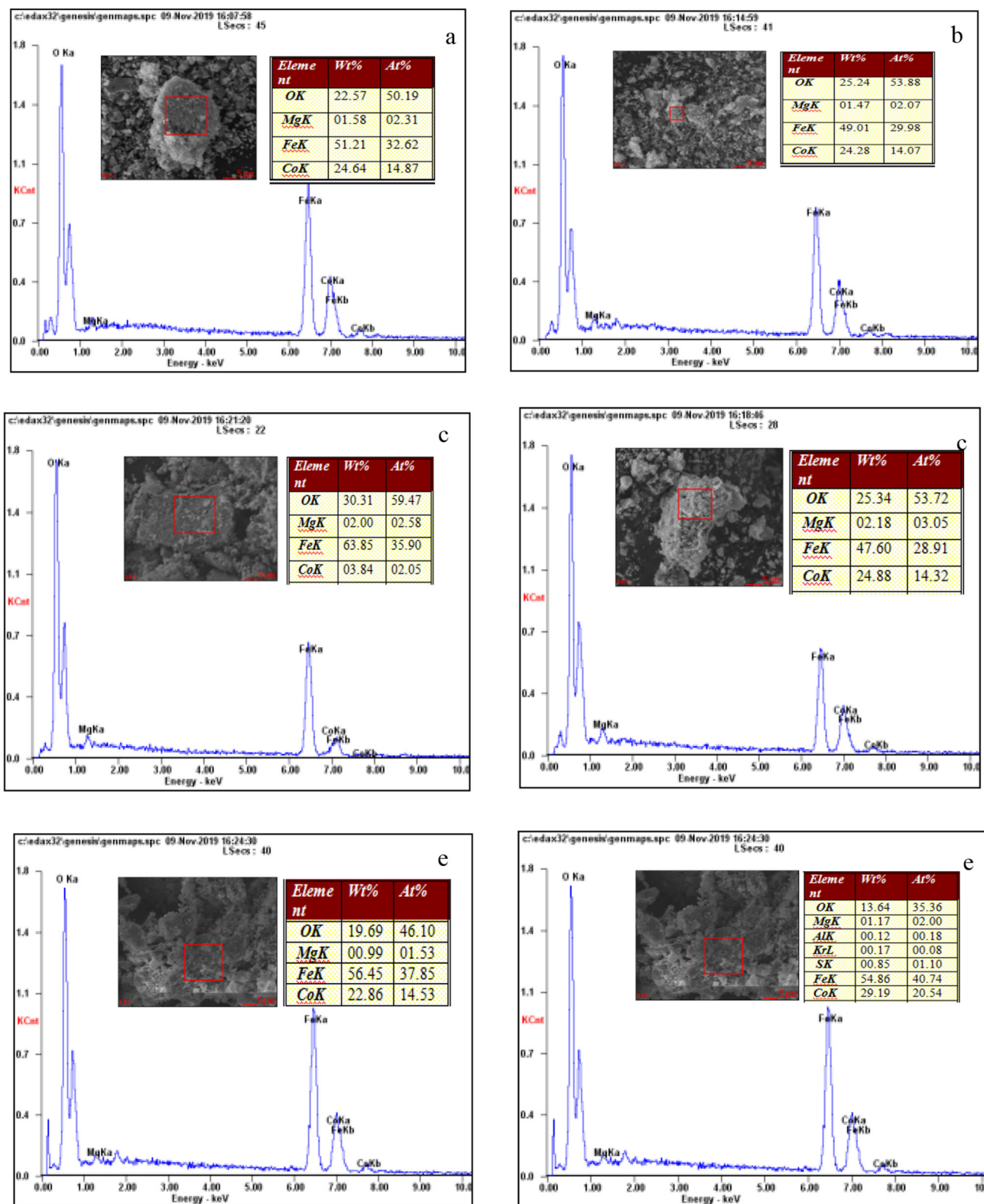


Fig. 5 EDS spectra of $Mg_{0.1}Co_{0.9}Fe_2O_4$ ferrite nanoparticles prepared using different complexing agents (**a** no complexing agent, **b** citric acid, **c** oxalic acid, **d** tartaric acid, **e** glucose, and **f** egg white)

value of multiple measurements is shown in Fig. 5. The calculation of each element content gives the chemical formula of the prepared sample which is approximate to $\text{Mg}_{0.11}\text{Co}_{0.88}\text{Fe}_{2.1}\text{O}_{4.8}$. The chemical element ratio of the sample is somewhat different from the target product. It may be due to the irregularity of the selected area of the sample component. In addition, since the prepared sample has a large number of pores and a relatively large porosity, the prepared sample will absorb a certain amount of oxygen on the surface, resulting in an excessive oxygen content. It is thus possible to initially determine the preparation of the sample as the target product.

3.5 Specific surface area test analysis (BET)

The specific surface area of magnesium–cobalt ferrite nanocrystals was measured by static nitrogen adsorption capacity method. Before measuring the specific surface area of the prepared sample, the sample was degassed under the condition of vacuum and $-197\text{ }^{\circ}\text{C}$ for 4 h to remove the original adsorbate on the solid surface, and then adsorbed with liquid nitrogen.

The nanoparticles prepared without complexing agent (annealed) have a specific surface area of $3.8771\text{ m}^2/\text{g}$ and an average pore diameter of 39.84 nm . The nanoparticles prepared using glucose as the complexing agent (annealed) have a specific surface area of $5.9122\text{ m}^2/\text{g}$ and an average pore diameter of 28.57 nm . Theoretically, the grain size is inversely proportional to the specific surface area, but in this experiment, the specific surface area of the prepared sample became larger as the grain size became larger. It may be due to the fact that the sample prepared by the addition of glucose has a strong magnetic property, causing a serious agglomeration of the sample. Many gaps are formed among the particles in the grains agglomeration which includes larger grains, while the smaller grains are agglomerated more closely and the gap among the particles becomes smaller and fewer.

3.6 Magnetic measurements (VSM)

The use of different complexing agents (citric acid, oxalic acid, tartaric acid, glucose, and egg white) to successfully prepare a magnesium–cobalt ferrite powder which has a spinel structure can be

demonstrated. This experiment mainly studies the effect of the type of complexing agent on the magnetic properties of ferrite. Therefore, the sample is characterized by the vibration sample magnetometer and the characterization results are shown in Fig. 6. The saturation magnetization, residual magnetization, and coercivity of the sample are different from those without the addition of complexing agent. Analysis of the shape of the hysteresis loop shows that the prepared samples belong to the hysteresis loop of the ferromagnetic material.

During the formation of the spinel ferrite, the divalent and trivalent metal cations occupy the octahedron (B position) and the tetrahedron (A position) in the spinel structure, respectively. The reason for the formation of positive magnetic spinel structure is that the octahedral position is occupied by trivalent metal ions and the tetrahedral position is occupied by divalent metal ions. The formation of inverse magnetic spinel structure is due to the fact that the octahedral position is occupied by divalent metal ions and the tetrahedral position is occupied by trivalent metal ions. The lattice structure model of the ferrite and the definition of the position of the octahedron and the tetrahedron are shown in Fig. 6.

We know that the magnetic properties of ferrite are derived from the spin of the surrounding electrons of the metal cation and the superexchange interaction between the metal cation and the oxygen ion. The interaction between the same cation and the oxygen ion is (A–A, B–B), and the interaction between the different metal cations and the oxygen ion is (A–B) [23]. Among these three exchange effects, the type of super-exchange of A–B is the strongest. Neel's ferromagnetic theory which describes the superexchange effect is shown in Fig. 7 [24, 25]. Physical properties of the prepared samples were measured by VSM (the test results are shown in Fig. 8) to obtain data, such as saturation magnetization, residual magnetization, and coercive force of the prepared samples (detailed data are shown in Table 4). The magnetic parameters were calculated in conjunction with the data given in Table 4 and the following formula, as shown in Table 5.

The formula is as follows [22]:

$$\mu_{\text{B(Cal.)}} = M_{\text{B}} - M_{\text{A}}, \quad (7)$$

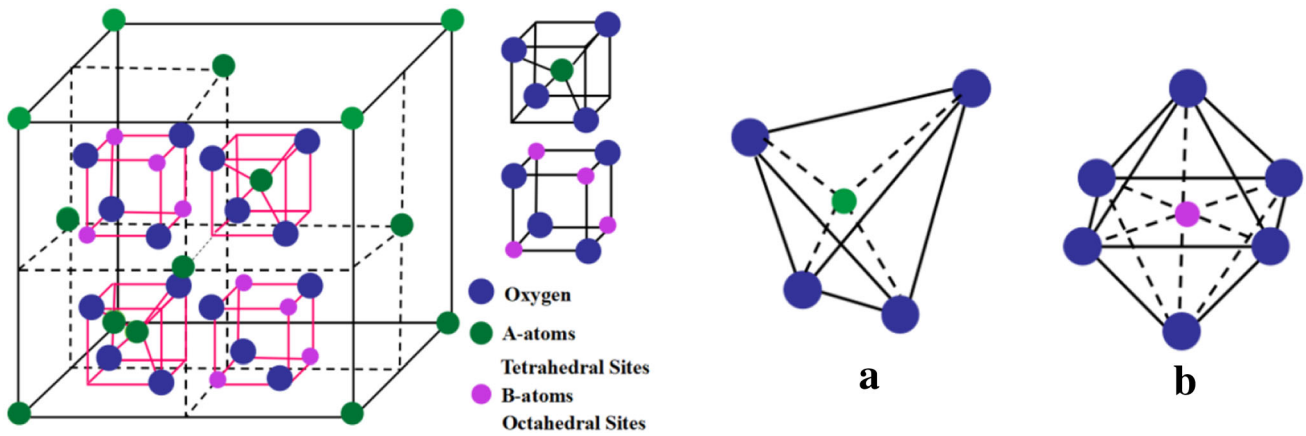


Fig. 6 Ferrites crystallize in the form of a cubic structure. Each corner of a ferrite unit cell consists of a ferrite molecule. **a** Tetrahedral or A sites and **b** octahedral or B sites

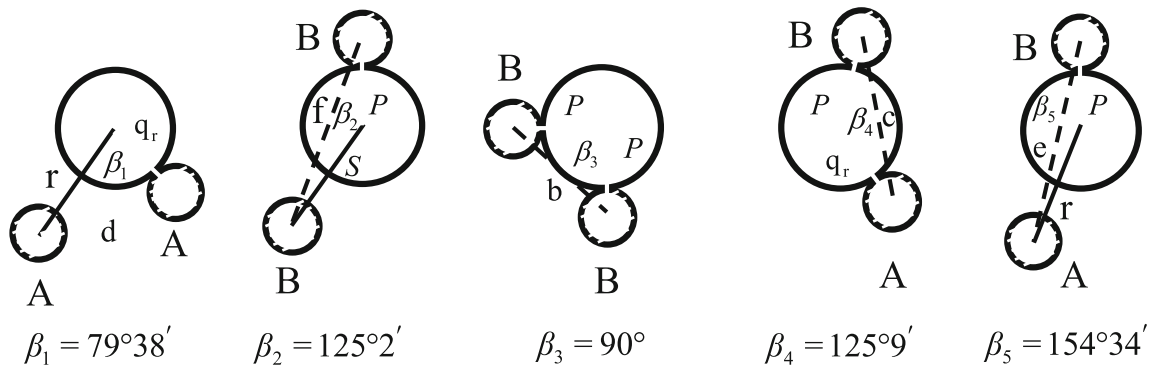
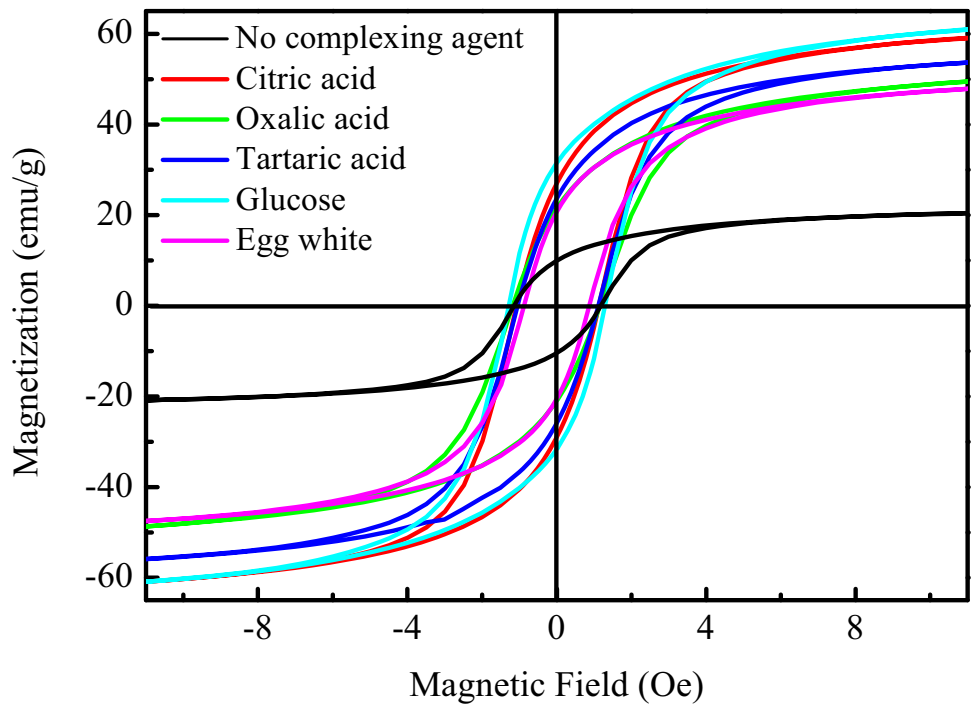


Fig. 7 Configuration of ion pairs in spinel ferrites with favorable distances

Fig. 8 *M–H* hysteresis loops of $Mg_{0.1}Co_{0.9}Fe_2O_4$ ferrite nanoparticles prepared using different complexing agents at room temperature



where μ_B is the total magnetic moment; M_A and M_B are the magnetic moments of the metal ion at the A and B positions, respectively [26].

$$\mu_{B(\text{exp.})} = \frac{M_w \times M_s}{5585}, \quad (8)$$

where M is the molecular mass of the corresponding ferrite, and M_s is the saturation magnetization of the corresponding sample [27].

$$H_c = \frac{2K}{\mu_0 \times M_s}. \quad (9)$$

The saturation magnetization M_s , coercive force H_c , and K are magnetic anisotropy constants.

Analysis of the data given in Tables 4 and 5 shows that the addition of a complexing agent to the reaction greatly enhances the magnetic properties of the sample, but the degree of effect of different complexing agents on the magnetic properties of the sample is different. Thus, the promotion on the magnetic properties of the sample is different, and when glucose acts as the complexing agent, the performance of the sample is increased the most. Glu-

Fig. 9 Field dependence of dM/dH of different samples. $2H_m$ measures the magnetic field that separates two peaks

cose acts as a complexing agent to increase the saturation magnetization of the sample from 20.836 to 61.512 emu/g, the residual magnetization from 10.19 to 31.58 emu/g, and the coercive force from 1128.24 to 1286.62 Oe. The anisotropy constant was also increased from 1.18×10^4 to 3.96×10^4 erg/g.

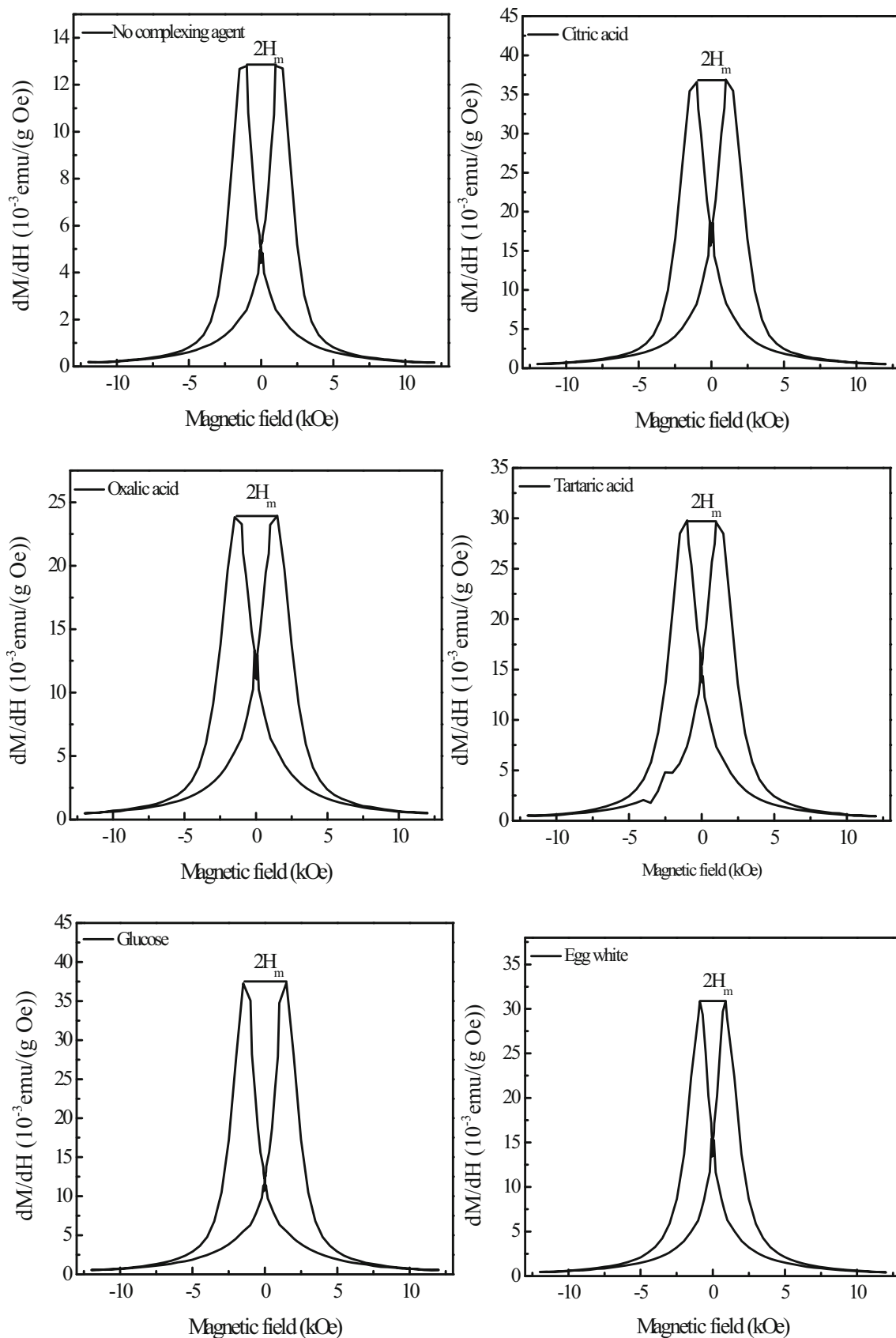
When glucose is used as the complexing agent, the gel mechanism is that the gel reacts with metal ions in the solution to form a complex, which is then calcined to be converted into magnesium–cobalt ferrite. The change of residual magnetization is mainly due to the fact that the use of different complexing agents changes optimum annealing temperature for each sample. On one hand, each sample annealed in the condition of heat preservation at 650 °C for three hours, resulting in different distribution of impurity and pore in the sample. The use of glucose as the complexing agent causes the magnetization inside

Table 4 Magnetic parameters of the prepared ferrite samples

Complexing agent	Remanent magnetization, M_r (emu/g)	Saturation magnetization, M_s (emu/g)	Coercivity, H_c (Oe)	Squareness, S (M_r/M_s)	Coercivity squareness S^*
No	10.19	20.836	1128.24	0.489	0.988
Citric acid	27.98	60.520	1102.73	0.462	0.246
Oxalic acid	21.25	49.611	1163.31	0.428	0.220
Tartaric acid	24.79	55.262	1074.98	0.463	0.354
Glucose	31.58	61.512	1286.62	0.449	0.101
Egg white	20.63	48.160	875	0.428	0.530

Table 5 Magnetic moment, magnetic anisotropy, dM/dH , and H_m calculated from $M(H)$ data for $\text{Mg}_{0.1}\text{Co}_{0.9}\text{Fe}_2\text{O}_4$

pH value	Unit cell magnetic moment $\mu_{B(\text{exp.})}$	Anisotropy constant $K \times 10^4$ (erg/g)	H_m (Oe)	dM/dH (emu/g/Oe) $\times 10^{-3}$	
				$H \rightarrow 0$	$H \rightarrow H_m$
No	0.86	1.18	997	5.04	12.8
Citric acid	2.50	3.34	991	16.346	34.26
Oxalic acid	2.05	2.89	1489	12.598	23.82
Tartaric acid	2.29	2.97	997	14.96	29.78
Glucose	2.55	3.96	1489	12.13	37.26
Egg white	1.99	2.11	896	14.98	30.86



the material to become relatively uniform, so that the demagnetizing field generated around the impurity and the pores is reduced, and thus, the residual magnetization becomes larger. On the other hand, since the addition of glucose sugar makes the impurities and pores uniform, the growth of magnetization reversal core is not easy so that the demagnetization process is in the first quadrant of the hysteresis loop, and the demagnetization nucleus becomes less to increase the residual magnetization.

In the process of adjusting the acidity of the solution with ammonia water, the metal ions in the solution, especially Fe^{3+} , first react with OH^- to form a yellow precipitate, and then the glucose is complexed with the formed metal precipitate to dissolve because of the difference of complexing constant. The complexing constant of glucose is the lowest; therefore, the distribution of metal ions in the xerogel obtained using glucose as the complexing agent is the most uneven, and the agglomeration is serious and the particle distribution is uneven when the particles are formed (this phenomenon can be observed in SEM). The grain boundary becomes thicker and the movement of domain wall becomes more difficult, resulting in a larger H_c of the resulting ferrite. When the sample is produced, the interaction of the crystal lattice changes due to the type of the complexing agent used, and thus, the anisotropy constant changes.

The dM/dH changes with the magnetic field at room temperature as shown in Fig. 9 and the dM/dH term represents the magnetic susceptibility of the magnetic material. For ideal single-domain particles in the hysteresis loop, the magnetic susceptibility is theoretically infinite (very large) when the magnetic field is H_c , and the magnetic susceptibility approaches zero when the magnetic field is zero. However, the experimental values differ greatly from the theoretical values and the data are shown in Table 5. This phenomenon further confirms the lattice structure of the monodomain/pseudo-monodomain and multidomain crystals in the studied sample [28, 29].

There are two peaks shown in Fig. 9 between which the distance is $2H_m$ and there is a difference between the peak height of the sample and the distance between the peaks ($2H_m$), because there are a large number of unstable superparamagnetic domains in the sample, and the amorphous phase which coexists in the lattice structure largely affects

the crystallization of the sample and thus causes a change in the performance of the sample.

4 Conclusions

A magnesium–cobalt ferrite of the formula $\text{Mg}_{0.1}\text{Co}_{0.9}\text{Fe}_2\text{O}_4$ was prepared by the sol–gel method. The nano-magnesium-cobalt ferrite powder which has a spinel structure and is relatively pure can be prepared without adding a complexing agent or changing the type of complexing agent (citric acid, oxalic acid, tartaric acid, glucose, and egg white). XRD and FTIR proved that the prepared sample has a good crystal spinel structure, and the purity of the sample is good. The addition of the complexing agent can change the microstructure of the sample. The SEM proves that the sample is granular or elliptical and the particle size is similar to the particle size calculated by XRD. It can also be seen that the sample particle size and distribution uniformity are different. The BET test shows that when a sample is prepared using glucose as the complexing agent, the specific surface area of the sample can be increased to enhance the adsorption capacity of the magnetic particles. VSM indicates that the addition of complexing agent to the reaction can greatly improve the magnetic properties of the samples, and when glucose is used as the complexing agent, $\text{Mg}_{0.1}\text{Co}_{0.9}\text{Fe}_2\text{O}_4$ ferrite with high magnetic properties can be prepared.

References

1. L. Bozadgiev, T. Dimova, T. Mitev, Classification of ferrospinel structures and textures. *J. Am. Ceram. Soc.* **68**(1), 1–12 (1985)
2. B. Geller, A. Coville, Magnetism and magnetic materials. *Phys. Today* **11**(6), 48–48 (1958)
3. S. Uday Bhasker et al., Preparation and characterization of cobalt magnesium nano ferrites using auto-combustion method. *Adv. Mater. Res.* **584**, 280–284 (2012)
4. N. Ranvah, Y. Melikhov, I.C. Nlebedim, D.C. Jiles, J.E. Snyder, A.J. Moses, P.I. Williams, Temperature dependence of magnetic anisotropy of germanium/cobalt cosubstituted cobalt ferrite. *J. Appl. Phys.* **105**, 5181–5183 (2009)

5. G.W. Coffey, J. Hardy, L.R. Pedersen, Electrochemical properties of lanthanum strontium aluminum ferrites for the oxygen reduction reaction. *Solid State Ion.* **158**, 1–9 (2003)
6. S.M. Abbas, A.K. Dixit, R. Chatterjee, Complex permittivity and microwave absorption properties of BaTiO₃-polyaniline composite. *Mater. Sci. Eng. B* **123**, 167–171 (2005)
7. M. Pardavi-Horvath, Microwave applications of soft ferrites. *J. Magn. Magn. Mater.* **215**, 171–183 (2000)
8. S.U. Bhasker, M.R. Reddy, Effect of chromium substitution on structural, magnetic and electrical properties of magneto ceramic cobalt ferrite nano-particles. *J. Sol-Gel Sci. Technol.* **73**, 396–402 (2015)
9. M.D. Osborne, M.E. Fleet, G.M. Bancroft, Next-nearest neighbor effects in the Mössbauer spectra of (Cr, Al) spinels. *J. Solid State Chem.* **53**, 174–183 (1984)
10. C.F. Zhang, X.C. Zhong, H.Y. Yu et al., Effects of cobalt doping on the microstructure and magnetic properties of Mn–Zn ferrites prepared by the co-precipitation method. *Physica B* **404**, 2327–2331 (2009)
11. J.A. Paulsen, C.C.H. Lo, J.E. Snyder, A.P. Ring, L.L. Jones, D.C. Jiles, Study of the Curie temperature of cobalt ferrite based composites for stress sensor applications. *IEEE Trans. Magn.* **39**, 3316–3318 (2003)
12. M. Srivastava, A.K. Ojha, S. Chaubey, P.K. Sharma, A.C. Pandey, Influence of pH on structural morphology and magnetic properties of ordered phase cobalt doped lithium ferrites nanoparticles synthesized by sol–gel method. *Sci. Eng. B* **175**, 14–21 (2010)
13. J. Jing, L. Liangchao, X. Feng, Structural analysis and magnetic properties of Gd-doped Li–Ni ferrites prepared using rheological phase reaction. *J. Rare Earths* **25**, 79–83 (2007)
14. S.K. Shinde, S. Ramesh, C. Bathula et al., Novel approach to synthesize NiCo₂S₄ composite for high-performance supercapacitor application with different molar ratio of Ni and Co. *Sci. Rep.* **9**, 13717 (2019)
15. R. Shen, C. Jiang, Q. Xiang, J. Xie, X. Lia et al., Surface and interface engineering of hierarchical photocatalysts. *Sci. Rep.* **5**, 3126–3134 (2018)
16. K. Siraj, M. Khaleeq-ur-Rahman, S.I. Hussain, M.S. Rafique, S. Anjum, Effect of deposition temperature on structural, surface, optical and magnetic properties of pulsed laser deposited Al doped CdO thin films. *J. Alloys Compd* **509**, 6756–6762 (2011)
17. G. Chandrasekaran, S. Selvandan, K. Manivannane, Electrical and FTIR studies on Al substituted Mn–Zn mixed ferrites. *J. Mater. Sci. Mater. Electron.* **15**, 15–18 (2004)
18. W.R. Agami, Effect of neodymium substitution on the electric and dielectric properties of Mn–Ni–Zn ferrite. *Physica B* **534**, 17–21 (2018)
19. M. Rahimi-Nasrabadi, M. Behpour, A. Sobhani-Nasab, S.M. Hosseinpour-Mashkani, ZnFe_{2–x}La_xO₄ nanostructure: synthesis, characterization, and its magnetic properties. *J. Mater. Sci. Mater. Electron.* **26**, 9776–9781 (2015)
20. N.S. Kumar, K.V. Kumar, Synthesis and structural properties of bismuth doped cobalt nanoferrites prepared by sol–gel combustion method. *World J. Nano Sci. Eng.* **5**, 140–151 (2015)
21. M. Ashokkumar, S. Muthukumar, Superlattices Microstruct. Zn_{0.96–x}Cu_{0.04}Fe_xO (0 < x < 0.04) alloys – Optical and structural studies. *Superlattices Microstruct.* **69**, 53 (2014)
22. P.A. Shaikh, R.C. Kambale, A.V. Rao, Y.D. Kolekar, Effect of Ni doping on structural and magnetic properties of Co_{1–x}Ni_xFe_{1.9}Mn_{0.1}O₄. *J. Magn. Magn. Mater.* **322**, 718–726 (2010)
23. V. Chaudhari, S.E. Shirsath, M.L. Mane, R.H. Kadam, S.B. Shelke, D.R. Mane, Crystallographic, magnetic and electrical properties of Ni_{0.5}Cu_{0.25}Zn_{0.25}La_xFe_{2–x}O₄ nanoparticles fabricated by sol–gel method. *J. Alloy Compd* **549**, 213–220 (2013)
24. L. Néel, Magnetic properties of ferrites: ferrimagnetism and antiferromagnetism. *Ann. Phys.* **3**, 137–198 (1948)
25. N.K. Dung, N.H. Tuan, The effect of cobalt substitution on structure and magnetic properties of nickel ferrite. *J. Sci. Math. Phys.* **25**, 153–159 (2009)
26. P. Anil Kumar, R. Mathieu, R. Vijayaraghavan, Subham Majumdar, Olof Karis, P. Nordblad, Biplab Sanyal, Olle Eriksson, D. D. Sarma, Magnetic properties of ferrites: ferrimagnetism and antiferromagnetism. *Ann. Phys.* **3**, 137 (1948)
27. J.M.D. Coey, Rare earth-iron permanent magnets. *Chem Inform* **23**, 236–241 (2010)
28. A.E. Berkowitz, J.A. Lahut, I.S. Jacobs et al., Spin pinning at ferrite-organic interfaces. *Phys. Rev. Lett.* **34**, 594 (1975)
29. I.P. Muthuselvam, R.N. Bhowmik, Mechanical alloyed Ho³⁺ doping in CoFe₂O₄ spinel ferrite and understanding of magnetic nanodomains. *J. Magn. Magn. Mater.* **322**, 767–776 (2010)

Publisher's Note Springer Nature remains neutral with regard to jurisdictional claims in published maps and institutional affiliations.